



JAAS

**A cavity ion source for high-precision isotope-ratio analyses
in the geosciences.**

Journal:	<i>Journal of Analytical Atomic Spectrometry</i>
Manuscript ID	JA-ART-05-2020-000228.R1
Article Type:	Paper
Date Submitted by the Author:	16-Jul-2020
Complete List of Authors:	Reimink, Jesse; The Pennsylvania State University College of Earth and Mineral Sciences, Geosciences; Carnegie Institution for Science, Earth and Planets Laboratory Carlson, Richard; Carnegie Institution for Science, Earth and Planets Laboratory Mock, Timothy; Carnegie Institution for Science, Earth and Planets Laboratory

SCHOLARONE™
Manuscripts

1 A cavity ion source for high-precision neodymium isotope-ratio analyses 2 in the geosciences.

3 Jesse R Reimink^{1,2}; Richard W Carlson², Timothy D Mock²

4 ¹Department of Geosciences, The Pennsylvania State University, University Park, PA, USA, 16803

5 ²Earth and Planets Laboratory, Carnegie Institution for Science, Washington, DC, USA, 20015

6 **Abstract:**

7 The principles governing ionization techniques used in thermal ionization mass spectrometers are
8 relatively well understood and have remained largely unchanged for many decades. Though significant
9 advances have been made in ion signal quantification for isotope ratio measurements, particularly for
10 analyses of small samples by using multiple detector systems and low-noise amplifiers, the fundamental
11 approach to sample ionization has received little focus. Modern TIMS techniques attempting to achieve
12 parts-per-million level isotope ratios precisions are realizing limits imposed by the physics of the
13 ionization source. A type of high-ionization efficiency thermal source employed in nuclear physics
14 communities for decades is the so-called cavity thermal ionization source. Here, we provide a proof-of-
15 concept study that shows cavity sources may provide a path forward to achieve a new level of precision in
16 isotope ratio measurements from solid samples. We document our new, simple, cavity ion source design,
17 show preliminary results from Nd isotope measurements, and discuss this new data in the context of
18 current precision limits imposed during traditional thermal ionization methods. We show that, within the
19 limits of our testbed mass spectrometer, mass fractionation within the cavity ion source appears similar to
20 that from filament ion sources. We also demonstrate that oxide-versus-metal ion production plays a
21 significant role in cavity ionization processes for Nd. Cavity ion sources may provide a viable path
22 forward to achieving isotope ratios precisions at the sub-ppm precision level.

23 **Introduction**

24 Mass spectrometers used to measure isotope ratios of geologic samples have long been standard
25 equipment in many geoscience laboratories. For the solid Earth geosciences, and geochronology in
26 particular, the thermal ionization mass spectrometer (TIMS) has been an essential tool. Thermal
27 ionization mass spectrometers are used to analyze the isotopic composition of a range of elements whose
28 first ionization potential is sufficiently low such that substantial ionization can occur before complete
29 sample evaporation from the filament (see Carlson, 2014 for a review). Multi-collector inductively

1
2
3 30 coupled plasma mass spectrometers (MC-ICPMS), introduced to the geosciences in the 1990's, use high-
4 31 temperature plasma sources that can readily ionize elements across the periodic table. At first MC-
5 32 ICPMS instruments were primarily used to analyze elements that were inefficiently ionized in a TIMS
6 33 instrument. Recently, ICP instruments have been used to analyze elements once thought to be securely
7 34 within the domain of TIMS procedures, such as Nd (Saji et al., 2016) and W (Archer et al., 2019) such
8 35 that the benefits of TIMS analyses become less apparent. ICP analyses are, however, not without their
9 36 downsides and TIMS instruments remain on the analytical cutting edge due to their comparative
10 37 simplicity of design, operation, and relatively simple mass spectrum. Both types of instruments appear to
11 38 be approaching roadblocks that limit the quest for increasing precision and sensitivity in isotope ratio
12 39 analyses. Overall efficiency, adopted here as the fraction of analyte atoms that end up being detected by
13 40 the mass spectrometer, is a major factor limiting both functional sample size and ultimate achievable
14 41 precision during isotope ratio measurements. Distinct hardware obstacles define the sensitivity limits in
15 42 ICP and TIMS, limits that are unlikely to be overcome without substantial redesign of the ionization and
16 43 ion transfer systems.

17
18
19 44 Though TIMS instruments have been, and remain, staples of Earth science facilities, they have
20 45 physical limits to their capabilities. In many cases, especially when dealing with small samples sizes or
21 46 very precise measurements, total efficiency proves to be the main limitation. This is because internal
22 47 precisions on isotope ratio measurements via TIMS often approach limits imposed by counting statistics
23 48 uncertainty (shot noise or Poisson noise). Lowering this barrier to higher precision will require counting
24 49 more ions either by increasing ionization efficiency, increasing measurement time, or both. The addition
25 50 of high-ohm feedback resistor amplifiers does not improve the precision on measurements of large ion
26 51 beams because ion counting statistics, not signal-to-noise ratio, is the limiting factor. Consequently,
27 52 advances in low-noise detection systems do not provide a path forward for these kinds of measurements.
28 53 Improvement is primarily needed on the front end of mass spectrometers to improve both the fraction of
29 54 atoms ionized and the efficiency of transmission of generated ions to the detector systems. In modern
30 55 TIMS instruments, the efficiency of ion transmission and detection can exceed 80% such that the highest
31 56 fraction of analyte atoms is lost during the evaporation and ionization process. However, ion sources
32 57 capable of producing a factor of 10-40 times more ions from a given amount of analyte compared to
33 58 conventional flat-filament TIMS sources have been developed, so-called thermal ionization cavity (TIC)
34 59 sources. Despite their obvious potential benefits, TIC ion sources have yet to achieve routine use in the
35 60 geosciences (see review in Maden et al., 2018). We have taken a new approach to the TIC source and
36 61 developed an ion source capable of analyzing large sample sizes at high ion beam intensities for long
37
38
39
40
41
42
43
44
45
46
47
48
49
50
51
52
53
54
55
56
57
58
59
60

1
2
3 62 durations with the goal of pushing precision limits below those currently possible with the traditional flat-
4 63 filament sources used in conventional TIMS.
5
6
7
8

9 64 **Current precision limits in TIMS analyses**

10 65 Standard TIMS instruments employ flat-filament ionizing surfaces wherein the analyte is loaded onto
11 66 a thin, flat strip of refractory high-work function metal. Ionization efficiency is improved for some
12 67 elements through the use of multiple filaments where one filament is kept at much higher temperature to
13 68 serve as an ionization surface for neutral atoms evaporated off of one or more “sample” filaments. The
14 69 flat-filament ionization assembly, though suitable for the vast array of TIMS applications, suffers from
15 70 two major drawbacks when considering achievement of parts-per-million isotope ratio precision.
16
17
18
19
20

21 71 First, in conventional TIMS flat filament sources, increasing sample size does not always translate to
22 72 proportionately longer runs or higher ion beam intensities. In fact, loading more analyte can decrease the
23 73 total efficiency (Edwards et al., 1987) such that e.g. a factor of two increase in sample size translates to
24 74 less than a factor of 2 increase in total ions counted. More problematical is that large sample sizes often
25 75 result in variable mass dependencies for the mass fractionation experienced during sample evaporation
26 76 and ionization, confounding attempts to accurately correct for that fractionation. These factors combine
27 77 to restrict our sample size to ~700 ng of Nd (Garçon et al., 2018; Reimink et al., 2018), much less than is
28 78 typically separated from an individual rock dissolution (~2 ug of Nd). A common explanation for the
29 79 fall-off in ionization efficiency for large samples suggests that large sample sizes limit the amount of
30 80 analyte in direct contact with the filament, thereby favoring evaporation over ionization. While possible,
31 81 making longer isotope ratio measurements, by pooling individual ~700 ng Nd loads from a single sample
32 82 dissolution, becomes increasingly time-inefficient; an analysis with 3-4 ppm internal precision already
33 83 requires 9-12 hours of continuous measurement of 4×10^{-11} A signals for $^{142}\text{Nd}^+$ (Horan et al., 2018; Peters
34 84 et al., 2018; Reimink et al., 2018).
35
36
37
38
39
40
41
42
43

44 85 The second major limitation in flat filament TIMS methods relates to the mass fractionation that
45 86 occurs during evaporation and ionization. At a basic level, mass fractionation during thermal ionization is
46 87 a straightforward and well-understood process (Habfast, 1983; Hart and Zindler, 1989; Russell et al.,
47 88 1978; Upadhyay et al., 2008). During evaporation and ionization, lighter isotopes are preferentially
48 89 removed from the solid phase such that the isotope ratios collected early in an analysis have a lower
49 90 heavy/light isotope ratio and this increases with time. This bias must be removed from the analysis, and is
50 91 often corrected by assuming that the fractionation is mass dependent and follows an exponential mass
51 92 dependency (Hart and Zindler, 1989; Russell et al., 1978). Although the exponential mass dependency is
52
53
54
55
56
57
58
59
60

1
2
3 93 simply an empirical fit to the observed mass fractionation in TIMS analysis, it has been shown to be
4 94 appropriate in the vast majority of TIMS analyses. However, in analyses requiring part per million
5 95 precision, the measured ratios can deviate from exponential law fractionation (Andreasen and Sharma,
6 96 2009; Garçon et al., 2018; Upadhyay et al., 2008). These measured deviations from exponential law are
7 97 typically interpreted as reflecting an ion beam that is derived from the combination of emission from a
8 98 number of variably fractionated reservoirs on a filament. This type of “mixing” imparts a linear, not
9 99 exponential, overprint on the otherwise exponential mass fractionation of isotope compositions
10 100 (Andreasen and Sharma, 2009; Fantle and Bullen, 2009; Garçon et al., 2018; Hart and Zindler, 1989;
11 101 Upadhyay et al., 2008). The exact mass dependency of the fractionation present in an ion beam derived
12 102 from an unknown number of reservoirs with an unknown extent of fractionation is impossible to
13 103 accurately correct. The problem is compounded in runs involving larger sample sizes as they more often
14 104 contain periods of complex mass fractionation during analysis. Thus, common practice involves removing
15 105 sections of an analysis that show clear signs of non-exponential mass fractionation (i.e., decreasing
16 106 heavy/light isotope composition with time) so as to avoid generating biases induced by inappropriate
17 107 mass fractionation correction (Andreasen and Sharma, 2009; Fantle and Bullen, 2009; Garçon et al.,
18 108 2018; Reimink et al., 2018; Upadhyay et al., 2008). This practice, however, may not completely account
19 109 for such effects that contribute to reproducibility at the parts-per-million level.
20
21
22
23
24
25
26
27
28
29
30

31 110 In this work, we explore the possibility that an alternative ion source design may overcome these
32 111 limiting factors and ultimately allow sub-ppm isotope ratio precisions. A suite of ion source designs has
33 112 been shown to generate ions at a rate many times higher than traditional TIMS methods (Beyer et al.,
34 113 1971; Johnson et al., 1973; Maden et al., 2018). These ion sources, which we will refer to as thermal
35 114 ionization cavity sources (TIC), have gained use in the nuclear physics and on-line isotope separator
36 115 communities but have never gained significant traction within the geosciences. The main limitations
37 116 include the complexity of the cavity designs along with the very high temperatures involved that stress
38 117 vacuum systems and exacerbate the need for ultrapure cavity materials in order to minimize background
39 118 signals. In this work we present a simple TIC ion source design that shows the potential for TIC to
40 119 produce very large ion beams for extended periods of time, with predicted precisions that are a necessary
41 120 prerequisite to push isotope ratio precision into the sub-ppm range.
42
43
44
45
46
47
48

49 121 In summary, isotope ratio precisions in the ppm range are limited by two main factors: 1) the number
50 122 of ions counted, and 2) variable mass fractionation behavior. As sample size increases in flat-filament
51 123 TIMS, ionization efficiency decreases and non-exponential mass fractionation increases. Both work in
52 124 the direction of leading to less precise isotope ratios.
53
54
55
56
57
58
59
60

125 **Previous cavity source designs**

126 Cavity ion sources were initially proposed in the 1970's (Beyer et al., 1971; Johnson et al., 1973) as a
127 method to achieve isotope separation of milligram-sized samples for nuclear studies. Since that time
128 many iterations have been developed, but to our knowledge only online isotope separators (Sato et al.,
129 2015) and one other geoscience laboratory (Trinquier et al., 2019) currently use the technology. A recent
130 publication (Maden et al., 2018) contains a thorough review of the development history of TIC sources.
131 Despite a wide variety of ionization geometries and mass analyzers, including magnetic sector (Bürger et
132 al., 2009; Li-hua et al., 2011; Maden et al., 2018; Trinquier et al., 2019), quadrupole (Duan et al., 1999,
133 1997), and time-of-flight analyzers (Wayne et al., 2001), all cavity ion sources share some similarities.
134 The essential components of TIC sources are a high-aspect-ratio cavity drilled into a high-work-function
135 metal such as Re, Ta, or W. Sample material is loaded into the rear of this cavity, which is then
136 electrically heated to high temperatures. Initial designs were simple and focused on generating large ion
137 beams from large samples for isotope separator laboratories (Beyer et al., 1971; Johnson et al., 1973), and
138 these forms of TIC sources remain in use among the nuclear physics community (Sato et al., 2015)
139 though typically used for smaller samples. However, recent TIC source developments have been driven
140 to achieve maximum ionization efficiency from very small (picogram) samples sizes of high ionization
141 potential elements (e.g., U, Pu, Am), usually driven by the analytical needs of the nuclear forensics
142 community (Bürger et al., 2007; Trinquier et al., 2019).

143 The physics of ionization in a cavity have been well-summarized (Kirchner, 1981; Maden et al.,
144 2016). The dominant mechanism of ionization at temperatures <2700 K, in typical-sized cavities, seems
145 to be thermal ionization from the cavity walls. This situation is similar to traditional flat-filament TIMS
146 sources, except that confined analyte atoms do not immediately escape the hot enclosure after
147 evaporation. Instead, any atom that evaporates, but does not ionize will likely come into contact with
148 another hot inner surface of the cavity. Thus, the proportion of atoms that eventually get ionized is
149 increased as each atom has many more opportunities to be ionized by thermal contact with hot cavity
150 walls. Maden et al. (2016) developed modeling code that accounted for space charge within the cavity
151 and showed that space charge along the cavity walls, dominantly derived from thermally-emitted
152 electrons, aids in ion extraction from the cavity. At temperatures above ~ 2700 K, a quasi-neutral plasma
153 may exist inside the cavity, thus increasing ionization (Kirchner, 1981) but potentially creating an
154 environment where ion movement becomes diffusive, thus changing extraction properties (Maden et al.,
155 2016). Independent of whether a quasi-plasma exists within a particular cavity design, TIC sources have
156 been shown to provide higher ionization efficiencies than traditional flat filament arrangements, with
157 ionization increases of up to a factor of 40 for elements of geologic interest. Despite decades of

1
2
3 158 development by many different laboratory research groups, TIC sources have never achieved routine use
4
5 159 in the geoscience community. Below, we highlight two recent cavity arrangements both aimed at
6
7 160 converting modern-style TIMS mass spectrometers to TIC sources for use in isotope ratio analyses and
8
9 161 summarize their results.

10
11 162 Driven by the goal of developing a mass spectrometer that could be quickly converted between a
12
13 163 cavity and flat-filament source, the research group at Oak Ridge National Laboratory employed a TIC
14
15 164 source first on a Finnigan MAT262 (Ingeneri et al., 2002; Riciputi et al., 2003), followed by installation
16
17 165 on a Thermo-Fisher Triton TIMS instrument (Bürger et al., 2009, 2007). This TIC geometry was created
18
19 166 by inserting an electrically insulated barrel within the commercial Triton barrel configuration. This new
20
21 167 inner barrel was held at the +10 kV operating voltage of the Triton instrument while the outer,
22
23 168 conventional barrel was stepped down to +8.5 kV. Cavity rods were mounted on the inner barrel such
24
25 169 that the conventional filaments, now held at -1.5 kV relative to the cavity rod, provided electron
26
27 170 bombardment current upon heating. In this way 21 cavity samples could be installed on a single modified
28
29 171 barrel yet the Triton software and data collection system remained unaffected by the presence of the
30
31 172 cavity ion source. Using this TIC setup, the Oak Ridge group showed that small (<10 ng) loads of Nd
32
33 173 and Sr could have total efficiencies approaching 20 – 30% (Bürger et al., 2009, 2007). However, the
34
35 174 stability and longevity of analytical runs were limited by alignment inefficiencies and arcing within the
36
37 175 source due to the complexity of the cavity arrangement. Additionally, the dramatic total efficiency
38
39 176 improvements found on the MAT262 instrument were apparently not seen on the Triton installation
40
41 177 (Bürger et al., 2009), perhaps due to the modification of the MAT262 ion lens system for cavity ion
42
43 178 beams (Ingeneri et al., 2002; Riciputi et al., 2003) and the design constraint that the Triton ion focusing
44
45 179 system remain unaltered for normal filament operations.

46
47 180 More recently, the research group at ETH Zurich has transitioned a multi-collector magnetic sector
48
49 181 mass spectrometer (Finnigan MAT262) to a TIC machine (Maden et al., 2018; Trinquier et al., 2019).
50
51 182 This design employs a dual-piece cavity assembly, a +10 kV accelerating voltage, and a cavity
52
53 183 arrangement that utilizes a flat carbon plate to prevent electrons from impacting the ion beam while
54
55 184 providing precise cavity location control. An additional advance is provided by a redesigned electrostatic
56
57 185 focusing lens stack and positional drive system capable of actively moving cavity tip location, aiding in
58
59 186 optimizing ion transmission. Thus far, the ETH TIC has produced total efficiency data on U (Maden et
60
187 al., 2018; Trinquier et al., 2019) analyses that showed >10 times improvement in the total efficiency
188
189 relative to flat-filament TIMS. The ETH TIC is distinct from the Oak Ridge design in that it can
190
accommodate only one cavity at a time, it contains a modified lens stack, and it uses larger cavity
dimensions. Nevertheless, the ETH source has produced total ionization gains relative to flat filament

1
2
3 191 TIMS that were better than the Oak Ridge Triton cavity setup (Bürger et al., 2009), but not substantially
4 192 improved from the initial Oak Ridge cavity installed on a modified Finnigan MAT262 (Ingeneri et al.,
5 193 2002; Riciputi et al., 2003).

8
9 194 Though cavity ion sources have shown substantial improvements in ionization efficiency (Maden et
10 195 al., 2016; Riciputi et al., 2003; Trinquier et al., 2019) in isotope ratio measurements they have yet to
11 196 become standard analytical tools in the geoscience community. The reasons for this are not entirely clear,
12 197 but what is evident is that most recent cavity ion source developments have focused on achieving utmost
13 198 efficiency from very small sample sizes. This analytical focus, though an obvious use for high-efficiency
14 199 cavities, suffers from competition with design improvements that allow for quantitative measurement of
15 200 small ion beam sizes (Koornneef et al., 2015) as the signal-to-noise ratio often dominates the uncertainty
16 201 budget of isotope ratio measurements of small samples using Faraday cup detectors. In the present work,
17 202 we take a different approach and focus on improvements that can be made to analyses where element
18 203 abundance is not the main limiting factor. Our aim is to use cavities to generate relatively large ($5e-10$
19 204 amp) ion beams from large sample sizes ($>1 \mu\text{g}$) and measure them for long periods of time (several
20 205 hours) to achieve isotope ratio precisions at the level of parts per million or better. This approach allows
21 206 us to relax design constraints aimed at peak ionization efficiency, such as operating cavities at very high
22 207 temperatures, that, in part, lead to some of the issues that have kept cavity ion sources from common use,
23 208 e.g. contamination of the source region by evaporated cavity material and background signals from
24 209 insufficiently pure cavity metals.

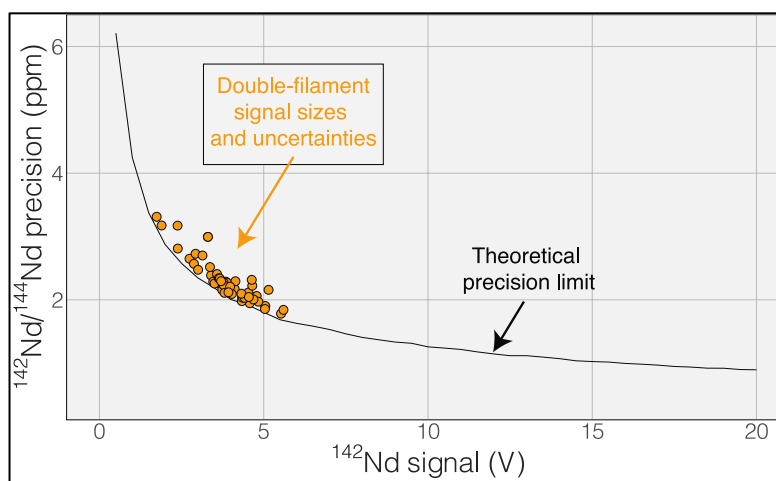
25 26 27 28 29 30 31 32 33 34 35 36 37 210 **Analytical background and approach**

38 211 The elements samarium (Sm) and neodymium (Nd) are extremely useful for the geoscience
39 212 community, as well as nuclear forensic (Krajko et al., 2014), applications. Particularly relevant to the
40 213 geosciences are the two radioactive isotopes of Sm, ^{146}Sm and ^{147}Sm , that undergo alpha decay to ^{142}Nd
41 214 and ^{143}Nd , respectively (Lugmair and Marti, 1977). Due to the slightly different chemical behavior of Sm
42 215 and Nd, the long-lived ^{147}Sm - ^{143}Nd decay system, with a half-life of ~ 106 billion years, has been widely
43 216 implemented in the geosciences community since the 1970's. The variations in $^{143}\text{Nd}/^{144}\text{Nd}$ induced by
44 217 radioactive decay of ^{147}Sm over geologic time are readily detectable with isotope ratio precisions of better
45 218 than 0.01%, making this system relatively easy to utilize with modern analytical systems. The other
46 219 decay system, ^{146}Sm - ^{142}Nd , has a much shorter half-life of ~ 103 million years and, due to the low
47 220 abundance of ^{146}Sm at the start of the Solar System, imparted much smaller variations in the daughter
48 221 isotope ratio $^{142}\text{Nd}/^{144}\text{Nd}$. Quantification of the variability in $^{142}\text{Nd}/^{144}\text{Nd}$ allows for detection of changes
49 222 in Sm/Nd during the lifetime of ^{146}Sm , lasting for the first 500 million years of Solar System history,
50
51
52
53
54
55
56
57
58
59
60

223 allowing for accurate chronology of Solar System materials (Marks et al., 2014), tracking of silicate
224 differentiation on Earth and other rocky solar system bodies (Boyet and Carlson, 2005; Carlson et al.,
225 2014; Harper and Jacobsen, 1992), and identification of Hadean reservoirs still present on the modern
226 Earth (Horan et al., 2018; Peters et al., 2018). These small $^{142}\text{Nd}/^{144}\text{Nd}$ variations are only detectable with
227 isotope ratio measurements that are precise at the parts-per-million level, as the total natural variation in
228 $^{142}\text{Nd}/^{144}\text{Nd}$ in Earth materials is only ~ 50 ppm. Thus, very precise isotope ratio measurements are
229 required to fully utilize the short-lived ^{146}Sm - ^{142}Nd system.

230 Modern precisions in the measurement of $^{142}\text{Nd}/^{144}\text{Nd}$ are on the order of 3-4 ppm (Garçon et al.,
231 2018; Peters et al., 2018; Saji et al., 2016). This level of precision requires measurement times on the
232 order of a dozen hours with beams around $5\text{e-}11$ amperes (equivalent to 5V on a $10^{11}\ \Omega$ resistor). As
233 shown by (Garçon et al., 2018), internal precision in the $^{142}\text{Nd}/^{144}\text{Nd}$ isotope ratio of multidynamic TIMS
234 measurements is only slightly poorer than the theoretical limits imposed by shot noise (Figure 1). This
235 means that the internal precision is chiefly dependent on the number of ions detected during a given
236 measurement.

237 *Figure 1: Uncertainty in*
238 *$^{142}\text{Nd}/^{144}\text{Nd}$ plotted as a function*
239 *of the average ^{142}Nd signal size*
240 *during a 6-hour analysis. The*
241 *actual measurements are shown in*
242 *orange and track the theoretical*
243 *limit imposed by shot noise*
244 *(Poisson noise), modeled using a*
245 *multi dynamic collection routine*
246 *that dramatically decreases the*
247 *impact of collector efficiency variations* (Garçon et al., 2018). *The close correlation between measured*
248 *and calculated uncertainty suggests that the uncertainty budget is dominated by shot noise such that*
249 *increasing signal size would be the most effective route to improving the internal precision of any given*
250 *analysis.*



251 While the internal uncertainty budget is dominated by shot noise, modern measurements achieve
252 internal precisions that push the limits of external reproducibility. In our experience, the external
253 reproducibility on modern double-filament Nd-isotope measurements remains ~ 4 -5 ppm, with
254 measurements of standards producing measured $^{142}\text{Nd}/^{144}\text{Nd}$ values that do not agree within the limits of

1
2
3 255 internal uncertainties. Our interpretation of this irreproducibility relies on observations of changing mass
4 256 fractionation, and deviations from exponential law, during any particular analysis (Figure 2). Though this
5 257 may seem to limit internal precision gains made by higher ion yields, cavity ion sources may provide a
6 258 means to more accurately quantify, and correct for, non-exponential mass fractionation and isobaric
7 259 interferences.

11
12 260 Mass fractionation during a TIMS measurement that deviates from exponential law is typically
13 261 interpreted to reflect an ion beam composed of a mixture of ions derived from sample regions on the
14 262 filament that have experienced different fractionation histories (Andreasen and Sharma, 2009; Fantle and
15 263 Bullen, 2009; Garçon et al., 2018; Hart and Zindler, 1989; Upadhyay et al., 2008), This process will vary
16 264 from analysis to analysis, potentially leading to significant external variability. The combination of ions
17 265 originating from variably fractionated sample domains on the filament will generate isotope ratio
18 266 deviations in predictable directions, calculated by considering the particular ratios used in mass
19 267 fractionation corrections. For instance, while using $^{146}\text{Nd}/^{144}\text{Nd}$ to correct $^{142}\text{Nd}/^{144}\text{Nd}$, mixing of the ions
20 268 emitted from variably fractionated domains on a filament will produce positive deviations from
21 269 exponential law, most easily visualized on a three-isotope plot (Andreasen and Sharma, 2009; Upadhyay
22 270 et al., 2008), creating an artificial increase in $^{142}\text{Nd}/^{144}\text{Nd}$. In fact, this type of behavior is readily
23 271 observable at the ppm precision level, as shown in Figure 2. During the analysis highlighted in Figure 2
24 272 (a typical analysis of JNdi standard solution from (Reimink et al., 2018)), data taken while the sample was
25 273 reversely fractionating (decreasing $^{146}\text{Nd}/^{144}\text{Nd}$ with time) have a $^{142}\text{Nd}/^{144}\text{Nd}$ ratio that is ~10 ppm higher
26 274 (+5.9 versus -3.3 relative to a $^{142}\text{Nd}/^{144}\text{Nd} = 1.141832$), on average, than the rest of the cycles measured
27 275 during the analysis. While the analysis shown in Figure 2 is readily filtered to remove portions of the
28 276 analysis that may be affected by non-exponential mass fractionation at the >15 ppm level, other, less
29 277 obvious, periods of such behavior within an analysis may not be so readily removed.

30
31
32
33
34
35
36
37
38
39
40
41
42
43
44
45
46
47
48
49
50
51
52
53
54
55
56
57
58
59
60

278

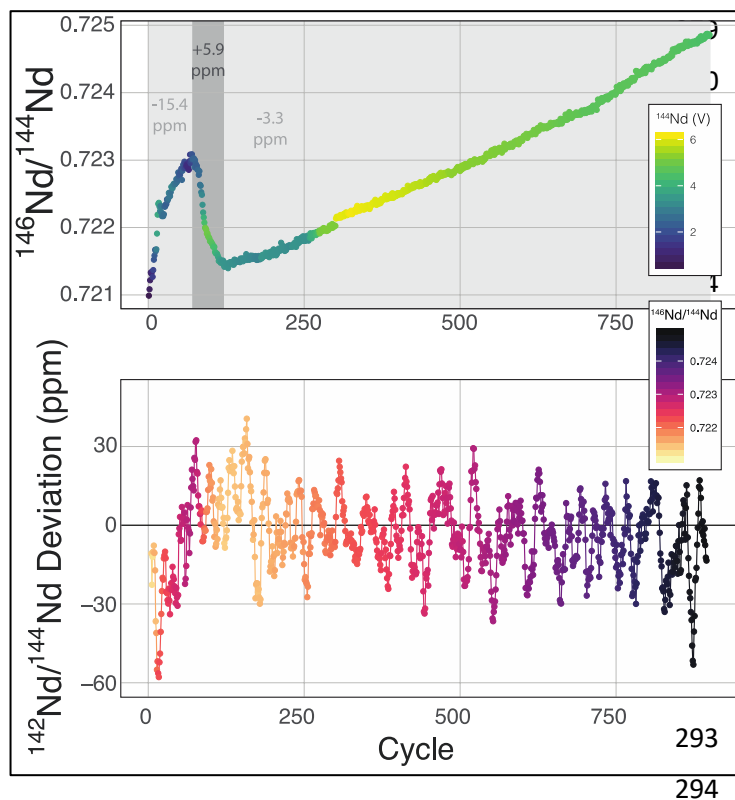


Figure 2: Mass fractionation during a single Nd-isotope measurement using the methods described in (Garçon et al., 2018). The top panel shows the measured $^{146}\text{Nd}/^{144}\text{Nd}$ ratio without mass fractionation correction as a function of the cycle number (each cycle is ~ 45 seconds with the total run lasting ~ 13 hours) with symbol colors corresponding to the ^{142}Nd signal size in volts across a $10^{11} \Omega$ resistor. The grey fields show three sections of the run, divided by fractionation trends, with the numbers indicating the average deviation from exponentially-corrected $^{142}\text{Nd}/^{144}\text{Nd}$ over that section of the analysis (all

fractionation corrected to an assumed $^{142}\text{Nd}/^{144}\text{Nd} = 1.141832$) The bottom panel shows a ten-point moving average of the deviation of each fractionation-corrected $^{142}\text{Nd}/^{144}\text{Nd}$ ratio from exponential law fractionation correction. Each measured $^{142}\text{Nd}/^{144}\text{Nd}$ ratio was time- and fractionation-corrected using a multi-dynamic collection scheme (Garçon et al., 2018), and then normalized to a $^{142}\text{Nd}/^{144}\text{Nd} = 1.141832$. The variably colored line connecting data points shows the sequence of cycles to aid interpretation.

Given the above considerations regarding precision and reproducibility during high precision Nd isotope analyses, we endeavored to implement a cavity ion source in a different manner than what has been attempted previously. Instead of optimal ionization from very small sample sizes, we aim to use the cavity ion source to generate large ($>5\text{e-}10$ A) Nd ion beams for long periods of time (several hours). Our development and design aimed to test whether cavity ion sources can provide a path towards sub-ppm Nd-isotope ratio precisions by, 1) generating large ion beams from large samples for long periods of time, thus driving down shot noise uncertainty, and 2) providing a means to more accurately correct for mass fractionation during TIMS analyses. Our approach and implementation thus allowed us to simplify a cavity ion source design as very high temperatures are not necessarily needed for our approach. This allows us to avoid engineering issues such as deposition of evaporated metal on insulators within the

1
2
3 310 source housing (Bürger et al., 2007) and controlling outgassing of the source components during high
4
5 311 temperature operation that may lead to high-voltage arcs (Maden et al., 2018).
6

7 312 The present work did not aim to produce higher total efficiencies than those achieved in modern
8
9 313 TIMS instruments as previous publications have clearly shown that cavity ion have sources the ability to
10
11 314 generate higher total efficiency for Nd than flat-filament TIMS (Bürger et al., 2007; Duan et al., 1999,
12
13 315 1997). Thus, we did not focus our design efforts on optimizing the ionization efficiency by, for instance,
14
15 316 testing a wide range of loading techniques or additives (Bürger et al., 2009; Trinquier et al., 2019), or by
16
17 317 substantially modifying the cavity dimensions; these improvements are clearly possible with cavity
18
19 318 ionization. Instead, we focused our design on testing whether large Nd⁺ ion beams can be generated for
20
21 319 long periods of time, producing total ion counting statistics that could drive down internal precisions.
22

23 320 **Cavity design**

24 25 321 *Mass spectrometer testbed and heating design*

26
27 322 Our cavity configurations were tested on a Carnegie-built single detector magnetic sector mass
28
29 323 spectrometer. This instrument is a 60-degree sector, 15-inch radius, Nier geometry magnetic sector mass
30
31 324 spectrometer with a single fixed faraday detector that can be moved to accommodate a secondary electron
32
33 325 multiplier. Ion beam intensities were measured by a Keithley 642 Electrometer, which was digitized
34
35 326 using a Keithley 2001 Digital Voltmeter and later by a Schumberger Solartron 7060 Systems Voltmeter.
36
37 327 All magnet control, data collection, and data reductions were performed using a custom LabVIEW
38
39 328 program written in-house.

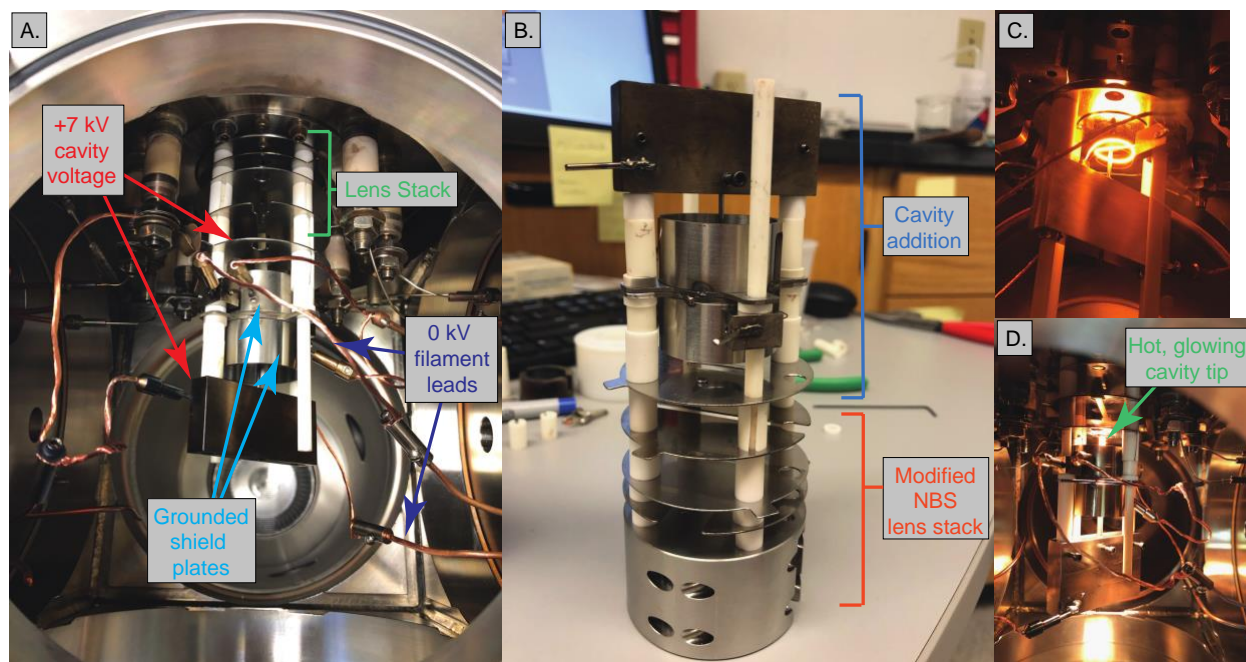
40
41 329 Our cavity ion source was heated using electron impact heating. This type of heating has been the
42
43 330 most common design implemented in TIC sources and we chose this design to avoid the requirement for
44
45 331 very large currents at high voltage required to resistively heat a cavity. A 0.4 mm diameter tantalum
46
47 332 filament was used as electron source and held at ground potential. Current was passed through this
48
49 333 filament using a Kepco JQE 0-50V, 0-10A power supply. Upon heating the filament provided an electron
50
51 334 current that impacted, and heated, the cavity source. The bombardment (heating) current was monitored
52
53 335 by the current absorbed by the cavity power supply and controlled manually. The voltage to the cavity
54
55 336 was provided by a Spellman SL2000 power supply capable of producing +15 kV at 110 mA. The
56
57 337 electron bombardment current was monitored by the Spellman power supply, where the current readings
58
59 338 were equivalent to the electron bombardment current from the grounded filament to the cavity. We
60
61 339 operated our cavity source at voltages between +5 to +7 kV. The electron bombardment currents during

1
2
3 340 an analysis scaled with the cavity voltage; heating power extended up to ~300 W, requiring 60 mA
4
5 341 bombardment current with a +5 kV cavity and 42 mA with a +7 kV cavity.
6

7 342 Two different ion optical lens systems were employed during our operation. The original lens system
8
9 343 on the 15-inch mass spectrometer is an NBS thin lens (Shields, 1966). This ion source consisted of
10
11 344 several lens elements made of 0.4 mm thick stainless steel with voltages provided by a resistor chain that
12
13 345 output voltages from +5 kV to ground. During our testing of the TIC source we determined that many of
14
15 346 the optical elements of the original lens system were likely unnecessary as they had little impact on
16
17 347 detected ion current across a range of voltage settings. Consequently, we simplified the lens system by
18
19 348 removing the discriminator and draw-out plates, keeping only x-focus and z-focus (y being the ion optical
20
21 349 axis) plates in addition to a defining plate and final collimating slits, all kept at the same dimensions as
22
23 350 the initial configuration. Data collected using this modified Shields source is presented in Table 1. This
24
25 351 configuration was, unfortunately, limited in its voltage range such that during many analyses the x- or z-
26
27 352 focus plates were at their maximum voltage difference, potentially limiting ion transmission. As a
28
29 353 potential improvement, we opted to test a second ion lens system. This second optical design was
30
31 354 modeled after a simplified lens system designed for a triple-filament ionizing source (Loveless and
32
33 355 Russell, 1969). In this Loveless and Russell source focusing system, only one set of four thick plate
34
35 356 electrodes is employed, along with a pair of grounded collimating slits as in the initial design. The four
36
37 357 electrodes are held at a potential close to the ionization source forcing the ions to follow damped
38
39 358 oscillatory paths that are focused at the collimating slit (Figure 4). We employed a slightly larger version
40
41 359 of the Loveless and Russell source design for several of our analyses (Table 1).
42
43
44
45
46
47
48
49
50
51
52
53
54
55
56
57
58
59
60

37 360 The 15-inch mass spectrometer ion extraction system is mounted on four ceramic rods (Figure 3A,B),
38
39 361 having a ~0.01 mm smaller bore than the lens plates, to prevent differential thermal expansion from
40
41 362 breaking the ceramic rods. In the case of both lens stack systems, we built the cavity ion source directly
42
43 363 out from this existing lens system such that our cavity source would be easy to position reproducibly in
44
45 364 the center of the lens system. A large, grounded, cylindrical shielding plate surrounded most of the hot
46
47 365 cavity to prevent cavity material from being deposited on the ceramic insulating rods. This shielding
48
49 366 plate also surrounded the electron bombardment filament through which the filament heating leads were
50
51 367 positioned. Finally, cavities were held by a stainless-steel block that was fixed to two of the ceramic
52
53 368 mounting rods extending from the lens stack (Figure 3). This block was held in place using set screws,
54
55 369 and the entire assembly was affixed to long ceramic rods mounted to a base block mounted inside the
56
57 370 source housing. Our cavity design left the cavity attached to the mount at its base, away from the
58
59 371 ionization tip. The stainless steel block was held snugly against ceramic tubes cut to length to maintain a
60
372 constant cavity y-position in front of the extraction lens system. Likewise, the cavity was held in the

373 stainless steel block with a set screw, and positioned manually using a measured mounting block such that
 374 the length of cavity sticking out in front of the stainless block was reproducible. However, the cavity
 375 ionization tip was freely floating, meaning that the cavity position may have changed during an analysis
 376 through sagging during high-temperature operation, altering the focal properties. Unfortunately, this
 377 sagging was only observable through a change in the lens stack voltages that achieved optimal ion
 378 transmission and was impossible to accurately quantify. This is distinct from the ETH design which fixes
 379 the ion source location by attaching the cavity tip to a graphite plate that controls the ion extraction
 380 location in x,y,z space (Maden et al., 2018).



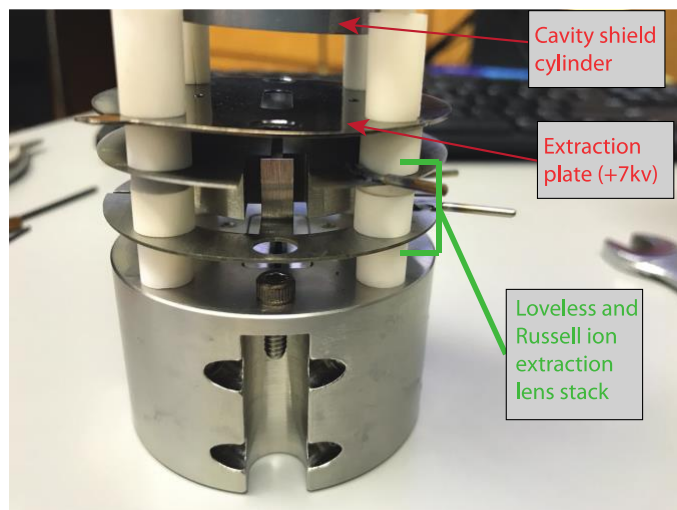
381
 382 *Figure 3: Images of the cavity ion source mounted on the Carnegie 15-inch single-collector instrument.*
 383 *A: The cavity ion source installed inside of the source housing of the 15-inch mass spectrometer with the*
 384 *modified Shields lens stack. B: the cavity assembly mounted on rods extended out from the modified*
 385 *version of the NBS lens stack. C: The cavity heated up without the shield plate in place so that the*
 386 *electron-emitting filament can be seen (the original, unmodified, NBS lens system is shown in this figure).*
 387 *D: The cavity under operating conditions, with the hot tip of the cavity visible and the electron-emitting*
 388 *filament hidden behind the shield plates. Note that this version had the tip of the cavity closer to the*
 389 *extraction lens plate than that shown in B. The performance characteristics were not detectably different*
 390 *between these two systems.*

391 During this work we used cavities made of Ta rod with a 3.1 mm outside diameter (supplied by H
 392 Cross company, 99.7% Ta). The cavities were made by electrical discharge machining 1.5 mm wide

1
2
3 393 holes into the Ta rod, creating cavities of various depths (10-40 mm; Table 1) and 1.5 mm diameters. The
4
5 394 diameters were chosen to match both the machining capabilities of the Carnegie machine shop and be
6
7 395 comparable to the dimensions of cavities recently shown to produce high ionization efficiencies in other
8
9 396 labs (Bürger et al., 2009; Maden et al., 2018). Tantalum was used as the cavity material during our
10
11 397 analyses due to the low cost and ease of machining relative to Re. Analyte Nd was loaded into cavities in
12
13 398 a 2M HCl solution containing 1ppm Nd using a 10 μ L syringe (Hamilton syringe 10 μ L, Model 701 RN
14
15 399 SYR, Part #7635-01). Carbon additive was loaded in the same manner using AquaDAG solution of
16
17 400 colloidal graphite. AquaDAG was loaded on top of dried down Nd sample at the base of the cavity.
18
19 401 During some analyses, Re powder was also added to the cavity to aid in ionization. Re powder (99.7 %
20
21 402 Re) was suspended in MilliQ water and ~2 μ L was loaded on top of the Nd HCl solution before drying.
22
23 403 For some analyses, cavities were re-used several times. While cavities were not completely cleaned of
24
25 404 Nd prior to loading another analysis, we are confident that only a small fraction of the total ions detected
26
27 405 may have come from prior sample loadings. This is due to several factors. First, we typically removed
28
29 406 and replaced the Re lining in between sample loads, which significantly reduced the amount of Nd
30
31 407 remaining in any previously used cavity. Also, we discovered that upon cooling a cavity and reheating,
32
33 408 the ion beam signal size would only return to significant size when it reached heating powers close to the
34
35 409 maximum power of the previous analysis. This means that as long as subsequent analyses remained at
36
37 410 heating power below the previous maximum, very little ionization of previous analyte occurred. We
38
39 411 attempted to clean cavities by boiling in 8M HNO₃ overnight, and subsequent ultrasonication, but this
40
41 412 appeared to only have a limited effect on presence of Nd in the cavity. More testing will need to be
42
43 413 accomplished to fully clean previously used cavities.

37
38 414 During the latter stages of our analysis, we lined the Ta cavities with Re foil to create a higher work
39
40 415 function surface on the inside of the cavity. The Re foil was 0.025 mm thick 99.7% pure Re foil from
41
42 416 Thermo-Fisher (#010307-FI), which was cut to size, wrapped around a post, inserted into the cavity, and
43
44 417 expanded to firmly contact the Ta cavity walls. After initial testing, we also inserted two Re filaments
45
46 418 (99.7% pure from H Cross) in a cross pattern into the base of the cavity before loading the cylindrical foil
47
48 419 lining so that analyte loaded into the bottom of the cavity would be loaded onto Re instead of bare Ta.
49
50 420 This was an attempt to further reduce NdO₊ production.
51
52
53
54
55
56
57
58
59
60

1
2
3 421 *Figure 4: An image of the Loveless and Russell ion extraction source system used in this work. In order*
4
5 422 *of top to bottom, the tip of the grounded cavity shield cylinder is exposed at the top of the image (with no*



6
7
8
9
10
11
12
13
14
15
16
17
18
19
20
21
22
23
24
25
26
27
28
29
30
31
32
33
34
35
36
37
38
39
40
41
42
43
44
45
46
47
48
49
50
51
52
53
54
55
56
57
58
59
60
cavity installed), followed by the +7 kV extraction plate, then the x-symmetry plates of the Loveless and Russell source, followed by the z-symmetry plates. The bottom block contains the two collimator slits and is the original part of the 15-inch mass spectrometer.

431

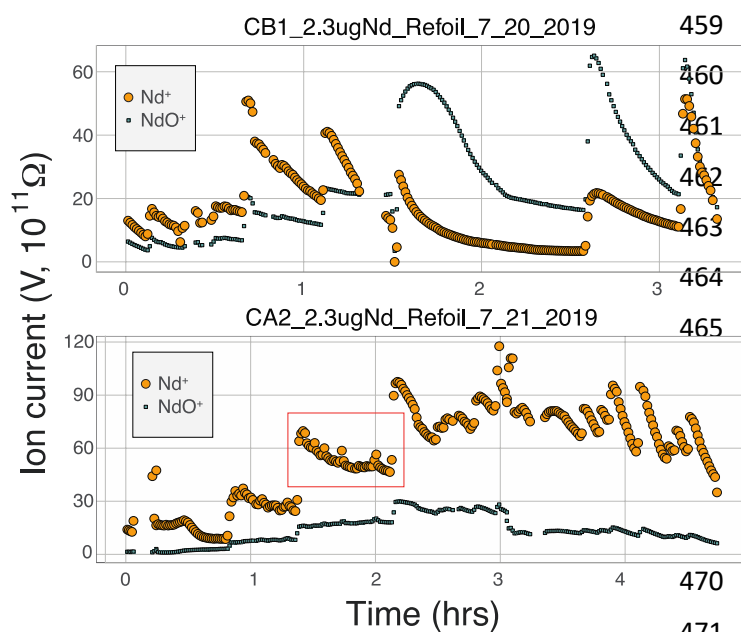
432 **Results and Discussion**

433 ***Signal size:***

434 During the course of our testing and analysis we focused on generating large ion beams of Nd⁺ for
435 long periods of time using cavity loads of 2 micrograms as we regularly separate 2 μg of Nd from
436 geological samples. A Nd⁺ signal was detectable on our faraday detectors when the heating power
437 approached ~80 W (~12 mA with +7 kV cavity voltage). Upon first appearance of a Nd⁺ beam, the signal
438 grew rapidly during initial heating before decreasing, all at a constant heating power. Ion beam tuning
439 was completed manually during heat up and before starting data collection. If signal sizes or isotope
440 ratios degraded during data collection, the run was aborted and the signal refocused and tuned. After this
441 initial signal increase, the signal size grew exponentially with increased bombardment current and
442 eventually stabilized. Once large signals were achieved, they began to slowly decay over time and
443 required an increase in the electron bombardment current to maintain the signal size. Overall, this
444 behavior is similar to the behavior of Nd⁺ during double filament analyses, suggesting that similar
445 processes govern the evaporation and ionization of Nd from the surface of the cavity.

446 Several of our runs produced ion beams >5e-10 amps that lasted for several hours (Figures 5, 7).
447 However, there was significant variability in the total efficiency of each run. The highest signal sizes
448 were all generated using the simplified Shields lens system. However, some runs using this lens system

449 produced low total ionization yields. These low intensity runs were conducted under sub-optimal ion
 450 focusing conditions, where the voltage difference on the x-focus or z-focus plates was at a maximum.
 451 This implies that optimum focus was not achieved, and some fraction of the ion beam was not being
 452 directed into the collimating slit, likely producing a substantial reduction in total ion yield. Our
 453 interpretation of the scatter in total ion yields using the simplified Shields source is that lower ion yields
 454 represent runs where the focusing properties of the ion source was not optimal and suffered ion
 455 transmission degradation. An added component to the variable efficiencies was the different cavity
 456 loading procedures used, as described previously. Though widely varying cavity dimensions were used,
 457 no systematic variation in ionization efficiency was observed that correlated with cavity depth. More
 458 testing is required to optimize this feature of the cavity design.



459 *Figure 5: Production of Nd⁺ and NdO⁺*
 460 *over the course of two analyses with high*
 461 *ion yields. Both measurements were*
 462 *made using the modified NBS lens*
 463 *system. The top analysis was made with*
 464 *a Ta cavity with Re foil lining only the*
 465 *cavity walls. The bottom analysis was*
 466 *made with a Ta cavity that had Re foil*
 467 *lining the walls as well as Re filaments in*
 468 *the bottom of the cavity and Re powder*
 469 *added to the sample solution during*
 470 *loading. Each step function increase in*
 471 *signal size corresponds to an increase in*

472 *the heating power.*

473 The difficulty associated with optimizing ion focusing during ionization from a cavity source has
 474 been highlighted in other work (Bürger et al., 2009; Maden et al., 2018). To test a new approach, and
 475 guided by modeling using the SIMION modeling software, we implemented a modified Loveless and
 476 Russell ion optics design (Loveless and Russell, 1969) that was shown to produce significantly higher ion
 477 transmission when using a triple-filament ion source arrangement. Our design of the power supply
 478 system allowed for independent determination of the top voltage of the four steering plates in the lens
 479 system, with each plate then separately tunable using a parallel resistor chain with ~300 V of range. Our
 480 experiments showed that the Loveless and Russell lens system had excellent ion beam steering
 481 capabilities and was insensitive to x-focus and z-focus setting; that is, the signal intensity was simple to

1
2
3 482 optimize and remained relatively constant throughout each analysis. The Loveless and Russell ion source
4 483 system was designed to have the steering plates held at a voltage close to the accelerating voltage (~5 V
5 484 lower than maximum), and our optimum peak shape and ion transmission occurred near the +5 kV
6 485 accelerating voltage of the cavity. However, the total efficiencies were substantially decreased with this
7 486 lens system compared to the modified NBS source (Table 1), indicating that overall ion transmission was
8 487 suboptimal. Our interpretation for suboptimal focusing is that the ion beam was not fully collimated and
9 488 focused at the defining slit such that only a small fraction of the defocused beam was transmitted through
10 489 the mass spectrometer, as evidenced by the relatively insensitivity to x and z voltage settings.

16
17 490 Regardless of the difficulties in ion focusing, our cavity ion source has shown a promising ability to
18 491 produce large ion beam sizes for long durations. When the total ion counts from our TIC source are
19 492 compared to flat-filament measurements, they predict sub-ppm precisions in the $^{142}\text{Nd}/^{144}\text{Nd}$ isotope ratio
20 493 (Figure 6). These promising results were obtained in spite of several limitations in our current approach.
21 494 As discussed above, our ion focusing systems suffered from suboptimal performance in both designs; the
22 495 modified shield lens could not achieve optimal focusing while our modified Loveless and Russell source
23 496 displayed a substantial decrease in ion transmission. We did not run the Nd loaded into our cavities to
24 497 exhaustion. Though signal sizes continued to decline near the end of analyses, substantial Nd ion beams
25 498 often remained upon termination of the analysis. We did not push the temperature on our cavity to the
26 499 extremes that might be possible, so our ionization efficiencies (Table 1) are minimum estimates. Given
27 500 the cavity ion source efficiency increase shown by other labs, substantial additional gains in total ion
28 501 yields certainly appear possible with our TIC source design if ion transmission is improved with a
29 502 modified focusing system and the cavities are run to higher temperature to exhaust the analyte.

30
31
32
33
34
35
36
37
38 503
39
40
41
42
43
44
45
46
47
48
49
50
51
52
53
54
55
56
57
58
59
60

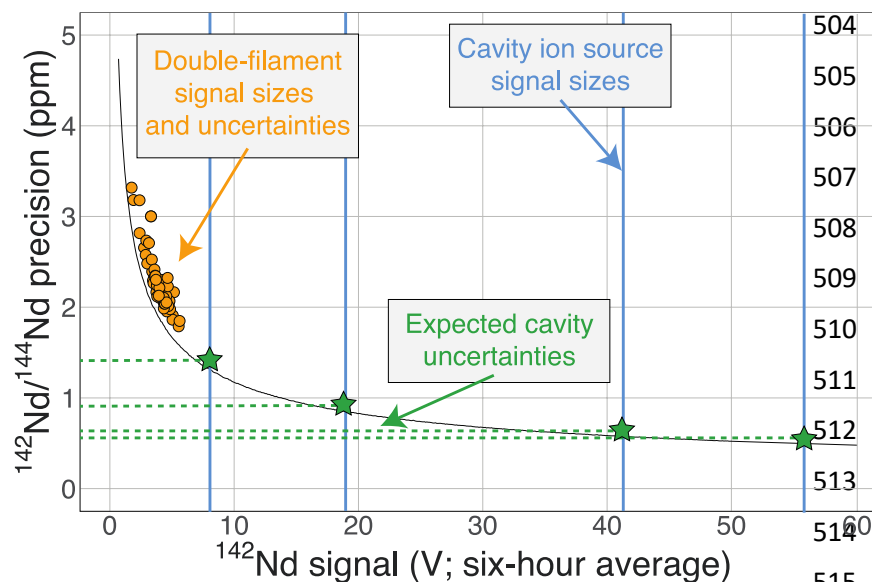


Figure 6: A modified version of Figure 1 showing the cavity ion yields. The average ^{142}Nd signal size in volts (relative to a $10^{11}\ \Omega$ resistor) during a 6-hour multi-dynamic Triton analysis (Garçon et al., 2018) is plotted against the internal precision achieved during that run (Reimink et al., 2018). The black curve is the

precision limit imposed by shot noise while the orange circles are actual double-filament analyses from samples and standards (Reimink et al., 2018). The vertical blue lines are total ion yields from the cavity ion source using $2\ \mu\text{g}$ of Nd (the highest signal size line was measured using $10\ \mu\text{g}$ Nd) converted to average signal size over six hours if these analyses were made on the Triton. The horizontal green dashed lines and stars are the predicted precisions of our cavity ion source analyses if mass fractionation corrections are similar, with the best analyses theoretically pushing the precision of the $^{142}\text{Nd}/^{144}\text{Nd}$ measurement below one part per million.

Neodymium oxide production

Many modern Nd isotopic analyses measure the metal ion, Nd^+ , though analyses of NdO^+ used to be common (Lugmair and Marti, 1977) and remain in use for analyses of very small analyses (Harvey and Baxter, 2009). The production of NdO^+ ions occurs at a lower temperature than the metal species, so higher ionization efficiency can be achieved when analyzing NdO^+ particularly when using an oxygen bleed valve or oxygen-emitter additives to the filament. Measurement of NdO^+ does not, however, provide a likely path towards more precise and accurate $^{142}\text{Nd}/^{144}\text{Nd}$ measurements as multiple isobaric interferences, and potential oxygen isotope fractionation during an analysis, must be accounted for when measuring polyatomic oxide species (Luguet et al., 2008).

To our knowledge, there has been only limited documentation of the various metal/oxide ion production abilities of Nd while using a cavity ion source, though metal/oxide production has been

1
2
3 535 investigated for other elements during short analysis times (<10 min (Maden et al., 2018; Trinquier et al.,
4 536 2019; Wayne et al., 2001)). Though colloidal carbon (AquaDAG) is often used during mass spectrometry
5 537 as a chemical reductant on the filament, the cavity community has also used carbon (either colloidal
6 538 graphite or organic resin bead loading) as an additive to increase the work function of the ionizer, in
7 539 addition to a chemical reductant, where ReC has a higher work function than Re metal (Bürger et al.,
8 540 2009; Maden et al., 2018). To evaluate the metal/oxide ionization within cavities, we tracked Nd^+/NdO^+
9 541 for the vast majority of our analyses. During most of our analyses, NdO^+ often had a higher signal during
10 542 the initial portions of the analyses, Re and C additives or a Re foil inside of the cavity aided in production
11 543 of Nd^+ (Table 1), optimizing ionization of the metal ion. During some analyses, however, NdO^+ was the
12 544 preferred species (Figure 5). The analysis shown in top panel of Figure 5 is from a cavity that was lined
13 545 with Re foil but did not have Re lining the base of the cavity. During the low-temperature beginning of
14 546 the analysis, Nd^+ is the dominant ion species, but in the middle of the analysis, NdO^+ becomes the
15 547 dominant species. One possible interpretation is that as temperatures increase NdO^+ begins to ionize
16 548 directly from the Ta base of the cavity, whereas at lower temperatures Nd evaporates as either metal or
17 549 oxide and is dominantly ionized as a metal during its multiple interactions with the cavity walls after
18 550 evaporation. An alternative interpretation invokes variable temperature along the cavity such that ions
19 551 may be extracted from the base of the cavity (as NdO^+) preferentially at the beginning relative to the later,
20 552 higher-temperature, portions of the analysis. The lower panel of Fig. 5 shows an analysis made with a
21 553 cavity that had Re foil covering the inner walls of the cavity as well as the bottom of the cavity and had
22 554 Re powder as an additive. During this analysis Nd metal ions are dominant throughout the entire duration
23 555 of the run, showing that limiting the exposure of analyte to the Ta cavity walls increased the metal
24 556 ionization efficiency.

25
26
27
28
29
30
31
32
33
34
35
36
37
38
39 557 In order to additionally decrease the NdO^+ production in our cavity designs we loaded colloidal
40 558 graphite (AquaDAG) along with Nd solution into the base of the cavities. This may have substantially
41 559 decreased the NdO^+ production from the cavity; average Nd^+/NdO^+ without AquaDAG is 4.7 and the
42 560 average with AquaDAG is 24.5 (Table 1), though these values are dominated by a few analyses and other
43 561 factors may play a role. This result suggests that the presence of a reductant (or Re powder) at the base of
44 562 the cavity has a significant influence over the Nd^+ production. (Bürger et al., 2009) documented a
45 563 dramatic increase in the ionization efficiency of Nd with either resin-bead loads or C additives from both
46 564 cavity ion sources and flat filament sources. They, however, interpreted this increase to be driven by the
47 565 increased work function of ReC, which aids in the ionization of all species. The impact of high-work-
48 566 function ReC was also invoked by (Maden et al., 2018) who interpreted an increase in U ionization over
49 567 the lifetime of individual Re cavities to be due to carbon from the graphite mounting plate diffusing into
50
51
52
53
54
55
56
57
58
59
60

the initially pure Re metal cavity. Our data show that, for Nd analyses, the competing ionization of Nd^+ and NdO^+ may play a dominant role over ReC as an ionizer. If formation of ReC was driving the Nd^+ ionization increase, metal ionization increases would be expected to match with greater production of NdO^+ due to the increased work function of ReC. Instead, the data suggest that at many times Nd^+ forms at the expense of NdO^+ and the two signals are inversely correlated during specific periods of the analyses. However, other more complex processes such as variable temperature distributions within the cavity may have a dramatic impact.

Mass fractionation

Our testbed mass spectrometer has only a single faraday detector so peak hopping was required to make isotope ratio measurements (typical data collection included $^{142}\text{Nd}^+$, $^{144}\text{Nd}^+$, $^{146}\text{Nd}^+$, $^{148}\text{Nd}^+$, $^{142}\text{Nd}_{16}\text{O}^+$, and $^{144}\text{Nd}_{16}\text{O}^+$, or some combination of these) therefore the isotope ratios are susceptible to ion beam intensity variations over the integration times used (between 4 and 10 seconds). Though all of our beam intensity data is time-corrected to the ^{144}Nd integration time by linear interpolation between two consecutive measurements of the isotope of interest, non-linear ion beam behavior can substantially bias resulting isotope ratios. Additionally, significant inconsistency in the ion beam intensity was produced during analyses, caused by several different factors. First, during initial manual heat-up the electron bombardment current was often manipulated to stabilize ionization, resulting in ‘jumps’ in ion beam currents that are not accounted for with a linear time-correction for ion beam intensity.

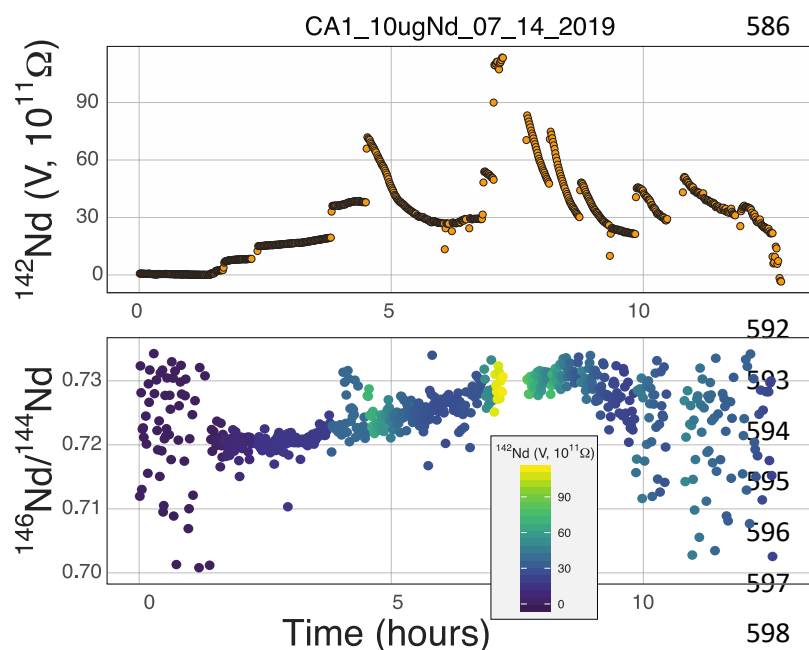


Figure 7: The signal size of $^{142}\text{Nd}^+$ during an analysis of a 10ug Nd load in a Ta cavity with C+Re additives (the NdO^+ signal stayed below 2V the entire analysis). The total ion yields from this run equate to a hypothetical precision of <0.5 ppm. The lower panel shows the mass fractionation throughout this run. Scatter in the isotope ratios are induced by step-function changes in ion beam intensity as well as instability in the

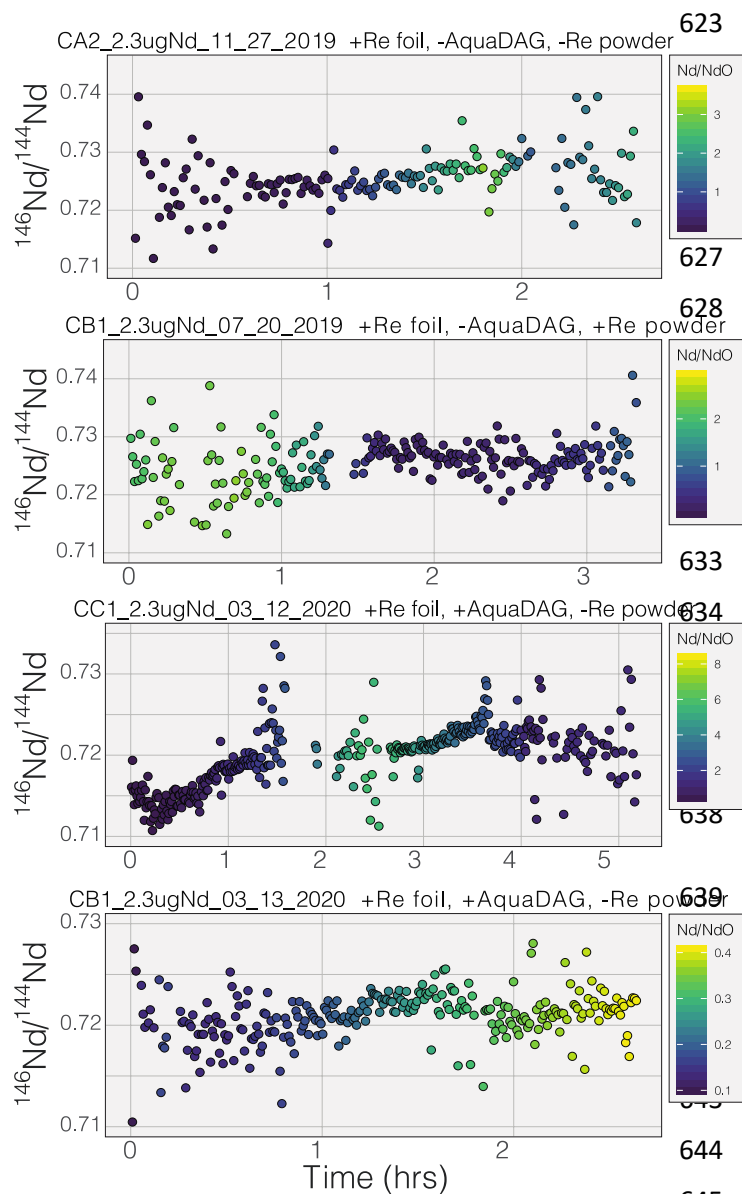
focusing system near the end of the analysis. This analysis shows mass fractionation that appears very

1
2
3 600 *similar, though of slightly greater magnitude, to double-filament analyses and contains no clear evidence*
4
5 601 *for complex fractionation behavior during the majority of the analysis, though the analysis has limited*
6
7 602 *isotope ratio precision for reasons laid out in the text.*

8
9 603 Second, particularly during analyses using the simplified NBS lens system at high temperature, the
10
11 604 resistor chain experienced voltage disturbances that created oscillations in the lens voltages. These
12
13 605 oscillations, likely due to electron currents to the front lens plate, resulted in ion beam variability on the
14
15 606 order of several volts with a periodicity of less than a second. This instability created most of the
16
17 607 instability in isotope ratios collected near the end of analyses using the NBS source (Figure 7). This
18
19 608 problem was eliminated during analyses with the Loveless and Russell ion optics system, which was
20
21 609 powered by an independent power supply instead of a resistor-divider chain.

22
23 610 Prior to this study, published mass fractionation behavior from cavity ion sources is limited to a
24
25 611 single, short-duration (~ 7 min) analysis of U (Maden et al., 2018) and one of Gd isotopes (Wayne et al.,
26
27 612 2001) though the latter may have been confounded by isobaric interferences. Potential shifts in mass
28
29 613 fractionation can substantially affect high precision isotope ratio measurements (Andreasen and Sharma,
30
31 614 2009; Garçon et al., 2018; Upadhyay et al., 2008). Similar to the Nd ion beam behavior, fractionation
32
33 615 from a TIC source (Figs. 7-8), at least to the precision allowed by our single-detector configuration (Figs
34
35 616 7-8), appears to be similar to mass fractionation from a double filament ion source (Fig. 2). The first
36
37 617 isotope ratios collected during an analysis had compositions lighter than the $^{146}\text{Nd}/^{144}\text{Nd} = 0.7219$ used as
38
39 618 the standard ratio for mass fractionation correction and showed 'normal' fractionation behavior
40
41 619 throughout the lifetime of an analysis, where the isotopic composition becomes heavier throughout the
42
43 620 run. The isotopic composition near the end of analyses reached a $^{146}\text{Nd}/^{144}\text{Nd}$ value that was similar to
44
45 621 that seen during flat filament analyses (0.730; (Garçon et al., 2018)), at which point the ion beam began
46
47
48
49
50
51
52
53
54
55
56
57
58
59
60

622 decaying substantially. Though we were not able to collect precise isotope ratios, there appeared to be no



623 relationship between Nd_+/NdO_+ ,
 624 and $^{146}Nd_+/^{144}Nd_+$ and, importantly, very
 625 little 'reverse' fractionation .

626 *Figure 8: The mass fractionation*
 627 *observed during four analyses of Nd. All*
 628 *isotope ratios are calculated from the*
 629 *metal species and the ^{146}Nd signal*
 630 *intensity is time-corrected for ion beam*
 631 *change to the ^{144}Nd integration by linear*
 632 *interpolation using the nearest two ^{146}Nd*
 633 *measurements. Symbol colors correspond*
 634 *to the Nd_+/NdO_+ during each integration,*
 635 *again time-corrected to the ^{144}Nd*
 636 *integration using linear interpolation.*
 637 *Note that the color scales are different in*
 638 *the four panels.*

639 Though no 'reverse' fractionation is
 640 detected in our cavity ion source analyses
 641 we do not have sufficient isotope-ratio
 642 precision to completely rule this
 643 phenomenon out ($^{142}Nd/^{144}Nd$ precisions
 644 were typically >40 ppm for a given run;
 645 Table 1). If cavity ion source

646 measurements do produce periods of non-exponential mass fractionation, the higher ion beam intensities
 647 provide a path towards correcting such behavior. The secondary y-axis in Figure 9 shows the within-
 648 integration standard deviations on the $^{142}Nd/^{144}Nd$ measurement using simple ion counting statistics and
 649 uncertainty propagation (and an 8-second integration time). The typical signal sizes achievable for our
 650 modern double-filament ^{142}Nd analyses (~ 4 V) are shown by the horizontal dashed line, which
 651 corresponds to a within-integration uncertainty of ~ 32 ppm, in excellent agreement with our multi-
 652 collector instrument observations (Reimink et al., 2018). As expected, the per-integration uncertainty of
 653 any isotope ratio dramatically decreases with signal size. If measurements of ion beam currents $\sim 5e-10$
 654 amps (50 V on a $10^{11} \Omega$ resistor) are made, the standard deviation on any given integration would drop to

655 ~9 ppm, allowing non-exponential fractionation effects to be resolved much more precisely (Figure 9).
 656 This calculation shows that even if cavity ion sources are susceptible to mass dependency fractionation
 657 variations during an analysis, they provide a path towards more accurate data by allowing for more
 658 precise filtering of integrations that have affected by this phenomena.

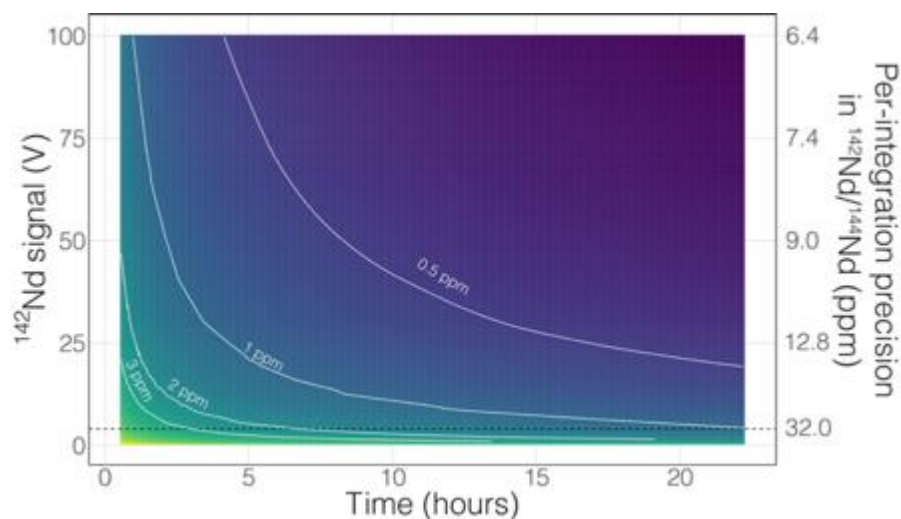


Figure 9: A simple calculation showing the total uncertainty in the $^{142}\text{Nd}/^{144}\text{Nd}$ ratio as a function of signal size and analytical times. The colors show precisions in the total $^{142}\text{Nd}/^{144}\text{Nd}$, with white curves highlighting precision contours. The

669 secondary y-axis shows the

670 within-integration (8-second integrations) $^{142}\text{Nd}/^{144}\text{Nd}$ standard deviation based on the Nd ion beam
 671 signal size. The horizontal dashed line indicates the typical 4 V $^{142}\text{Nd}^+$ signal reached in double filament
 672 ion sources, which have standard deviations ~32 ppm. We show that cavity ion sources are capable of
 673 generating >50 V Nd^+ ion beams for several hours, though such results are not standard in our suite of
 674 analyses and more work is required to make such analyses routine. Such large beams would allow for
 675 more precise tracking of non-exponential fractionation behavior during an analysis (with internal
 676 standard deviations <10 ppm), providing a path towards more accurate isotope ratios.

677 There are also more obvious benefits to the higher beam sizes that cavity ion sources will provide
 678 over traditional flat filament sources. First, there is the clear time-savings in that higher signal sizes
 679 achieve desired precision more quickly than small beams. This is shown in Figure 9 with a calculation
 680 that models the uncertainty of the fractionation-corrected $^{142}\text{Nd}/^{144}\text{Nd}$ as a function of analytical time and
 681 signal size. As expected, there is a decreasing precision return over time meaning that each additional
 682 hour of data collection achieves less of a relative precision increase than the last hour. The current state-
 683 of-the-art TIMS analyses for ^{142}Nd , measuring 4 V signals for 9-12 hours, are reaching a point where time
 684 quadrupling the analytical time to double the precision is becoming inviable. Even if analyzing a 4 V
 685 beam for 25 hours was possible, the precision increase would only be on the order of a few tenths of ppm
 686 in the isotope ratio precision. However, analysis of a 50 V beam for a ~2 hours will achieve internal
 687 precisions much lower than can be achieved currently. Thus, analyses at the same, or better, precision

1
2
3 688 level could be achieved in less than half the time. Analyses of 50V beams for this length of time with
4 689 double filament assemblies have not been shown to be possible, so cavity ion sources provide a new path
5
6 690 forward.
7

8
9 691 Finally, the higher ionization efficiency and signal sizes achievable with cavity ion sources will
10 692 provide more accurate and readily quantifiable interference corrections. This utility can, once again, be
11 693 illustrated with ^{142}Nd measurements. The main interfering elements of concern during ^{142}Nd
12 694 measurements are Ce (with an interference of ^{142}Ce on the Nd isotope of interest) and Sm (with several
13 695 isobaric interferences on important Nd isotopes). Accurately detecting any interfering element is a major
14 696 concern when dealing with isobaric interferences on isotope ratios measured at the ppm precision level.
15 697 Figure 10 shows the effect of signal size on detecting, and accurately correcting, potential interferences.
16 698 To correct the isobaric ^{142}Ce interference, ^{140}Ce is measured and a $^{142}\text{Ce}/^{140}\text{Ce}$ ratio of 0.12565 is assumed.
17 699 This correction is on the order of five ppm with a $^{140}\text{Ce}/^{146}\text{Nd}$ of 6.3×10^{-5} and falls with decreasing
18 700 Ce/Nd. Figure 10 shows two lines that calculate the ^{140}Ce signal at a given ppm correction in $^{142}\text{Nd}/^{144}\text{Nd}$
19 701 with varying $^{140}\text{Ce}/^{146}\text{Nd}$. When measuring Nd isotope compositions in Faraday detectors attached to
20 702 amplifiers equipped with $10^{11} \Omega$ resistors, a $50 \mu\text{V}$ signal is difficult to accurately quantify. If the ^{142}Nd
21 703 ion beam is 4 V, a ^{140}Ce signal of $50 \mu\text{V}$ would relate to a correction of -1.5 ppm, meaning that
22 704 interferences below ~ 1.5 ppm corrections will not be accurately quantified. With a 50 V ^{142}Nd beam,
23 705 however, a $50 \mu\text{V}$ ^{140}Ce signal will only represent a 0.1 ppm correction on $^{142}\text{Nd}/^{144}\text{Nd}$. Thus, higher
24 706 signal sizes will allow us to more accurately correct for interferences, even if such interferences are not
25 707 reduced by cavity measurements. Although lower noise faraday amplifiers are finding increasing use in
26 708 the detection of small interferences, the use of such amplifiers in combination with relatively low gain
27 709 amplifiers complicates multi-dynamic measurement schemes that switch ion beams between different
28 710 faradays in order to compensate for inefficient ion retention.
29
30
31
32
33
34
35
36
37
38
39
40

41
42 711 As well as the obvious need to accurately quantify any interfering signal, the unknown state of mass
43 712 fractionation of Ce and Sm leads to uncertainty in the amount of signal correction to be applied (Garçon
44 713 et al., 2018). Garçon et al. (2018) showed that for a ^{142}Nd analysis, the unknown fractionation state of
45 714 interfering elements adds excess uncertainty at the ~ 5 ppm level with $^{140}\text{Ce}/^{146}\text{Nd} > 1.6 \times 10^{-3}$ and
46 715 $^{147}\text{Sm}/^{146}\text{Nd} > 1.2 \times 10^{-4}$. These decrease to $^{140}\text{Ce}/^{146}\text{Nd} > 0.3 \times 10^{-3}$ and $^{147}\text{Sm}/^{146}\text{Nd} > 0.2 \times 10^{-4}$ when
47 716 considering measurements with 1 ppm precision. More precise quantification of the interfering elements,
48 717 even if their relative signals compared to the analyte of interest, can lead to more accurate application of
49 718 interference corrections, especially if quantification of mass fractionation of the interfering elements can
50 719 be achieved by, for instance measurement of $^{147}\text{Sm}/^{149}\text{Sm}$ ratios during the analysis. Higher signals will
51
52
53
54
55
56
57
58
59
60

720 clearly allow for more precise and accurate interference corrections, even if for instance the Nd/Sm ratio
 721 were to stay the same, leading to more accurate data.

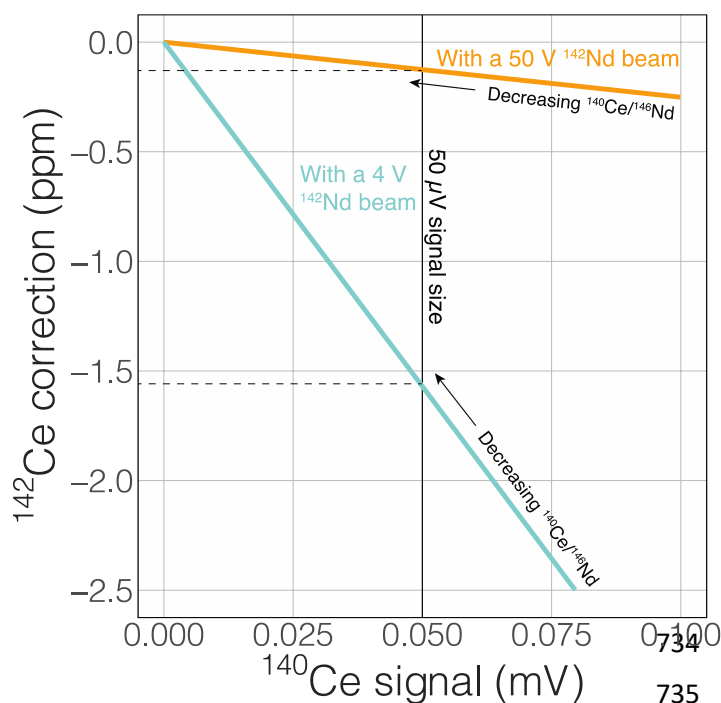


Figure 10: The magnitude of correction for the isobaric interference of ^{142}Ce on the ^{142}Nd measurement as a function of the ^{140}Ce signal and varying Ce/Nd ratios. Two lines are shown, one with a 50V ^{142}Nd beam and the other with a 4V beam. All calculations were made assuming measurement on a Faraday cup and amplifier equipped with a $10^{11} \Omega$ resistor. A larger Nd signal will allow for more precise detection and application of important interferences, even if such interferences are not reduced. The same logic and calculations can be applied to

736 many different types of analyses. Note that at the same ^{140}Ce

737 Conclusions:

738 We present a proof-of-concept cavity thermal ionization mass spectrometer (TIC) ion source that
 739 could be used to achieve very high isotope ratio precision for large (microgram) sample sizes. Modern
 740 Nd-isotope analyses are currently limited to precisions of ~4-6 ppm due to counting statistics and non-
 741 exponential mass fractionation effects. We have developed a cavity ion source, heated by electron
 742 bombardment, that is capable of producing $> 5e^{-10}$ amp (50 V on a $10^{11} \Omega$ resistor) Nd^+ ion beam sizes for
 743 several hours. Though more development is required to make these highly productive analyses routine,
 744 the expected precision from these cavity ion source analyses, when measured using modern multi-
 745 collector instruments, based on shot-noise limitations alone can approach 0.5 ppm for the isotope ratio of
 746 interest, $^{142}\text{Nd}/^{144}\text{Nd}$. We show that generation of large ion beams is possible from TIC sources and that
 747 the metal to oxide ratio, Nd^+/NdO^+ , plays a major role in the total ionization of Nd^+ from a TIC source.
 748 This ratio can likely be optimized using a combination of Re ionizing material and carbon additives, the
 749 latter serving as a reductant at the ionizing surface. Although our single-detector testbed mass
 750 spectrometer is not capable of making precise isotope ratio measurements, we show that mass
 751 fractionation from a TIC ion source appears to be similar to double filament sources. An improvement in

1
2
3 752 precision to sub-ppm levels in Nd-isotope ratios would allow full utilization of the paired $^{146,147}\text{Sm}$ -
4 753 $^{142,143}\text{Nd}$ decay systems and produce a significant advance in the understanding of early Solar System
5
6 754 events on Earth and other rocky bodies.
7
8
9

10 755 **Acknowledgements:**

11
12 756 This work was funded by an NSF EAR-IF grant to RWC and JRR (#1758571). The authors thank
13
14 757 Colin Maden with help in setting up Simion models that informed earlier design decisions. Joshua Davies
15 758 is thanked for enlightening comments and discussions. Mary Horan and Steve Shirey are thanked for
16
17 759 assistance in various stages of mass spectrometer setup and troubleshooting.
18

19
20 760
21
22
23
24
25
26
27
28
29
30
31
32
33
34
35
36
37
38
39
40
41
42
43
44
45
46
47
48
49
50
51
52
53
54
55
56
57
58
59
60

761 **References:**

- 762 Andreasen, R., Sharma, M., 2009. Fractionation and mixing in a thermal ionization mass spectrometer
763 source: Implications and limitations for high-precision Nd isotope analyses. *International Journal of*
764 *Mass Spectrometry* 285, 49–57. <https://doi.org/10.1016/j.ijms.2009.04.004>
- 765 Archer, G.J., Brennecka, G.A., Gleißner, P., Stracke, A., Becker, H., Kleine, T., 2019. Lack of late-
766 accreted material as the origin of ^{182}W excesses in the Archean mantle: Evidence from the
767 Pilbara Craton, Western Australia. *Earth and Planetary Science Letters* 528, 115841.
768 <https://doi.org/10.1016/j.epsl.2019.115841>
- 769 Beyer, G.J., Herrmann, E., Piotrowski, A., Raiko, V.J., Tyrroff, H., 1971. A new method for rare-earth
770 isotope separation. *Nuclear Instruments and Methods* 96, 437–439. [https://doi.org/10.1016/0029-](https://doi.org/10.1016/0029-554x(71)90613-6)
771 [554x\(71\)90613-6](https://doi.org/10.1016/0029-554x(71)90613-6)
- 772 Boyet, M., Carlson, R.W., 2005. ^{142}Nd evidence for early (>4.53 Ga) global differentiation of the silicate
773 earth. *Science* 309, 576–581. <https://doi.org/10.1126/science.1113634>
- 774 Bürger, S., Riciputi, L.R., Bostick, D.A., Turgeon, S., McBay, E.H., Lavelle, M., 2009. Isotope ratio
775 analysis of actinides, fission products, and geolocators by high-efficiency multi-collector thermal
776 ionization mass spectrometry. *International Journal of Mass Spectrometry* 286, 70–82.
777 <https://doi.org/10.1016/j.ijms.2009.06.010>
- 778 Bürger, S., Riciputi, L.R., Turgeon, S., Bostick, D., McBay, E., Lavelle, M., 2007. A high efficiency
779 cavity ion source using TIMS for nuclear forensic analysis. *Journal of Alloys and Compounds*
780 444–445, 660–662. <https://doi.org/10.1016/j.jallcom.2006.11.019>
- 781 Carlson, R.W., 2014. *Thermal Ionization Mass Spectrometry, Treatise on Geochemistry*. Elsevier.
- 782 Carlson, R.W., Borg, L.E., Gaffney, A.M., Boyet, M., 2014. Rb-Sr, Sm-Nd and Lu-Hf isotope
783 systematics of the lunar Mg-suite: the age of the lunar crust and its relation to the time of Moon
784 formation. *Philosophical Transactions of the Royal Society of London. Series A, Mathematical*
785 *and Physical Sciences* 372, 20130246–20130246. <https://doi.org/10.1098/rsta.2013.0246>
- 786 Duan, Y., Chamberlin, E.P., Olivares, J., 1997. Development of a new high-efficiency thermal ionization
787 source for mass spectrometry. *International Journal of Mass Spectrometry and Ion Processes* 161,
788 27–39. [https://doi.org/10.1016/s0168-1176\(96\)04434-5](https://doi.org/10.1016/s0168-1176(96)04434-5)
- 789 Duan, Y., Danen, R.E., Yan, X., Steiner, R., Cuadrado, J., Wayne, D., Majidi, V., Olivares, J.A., 1999.
790 Characterization of an improved thermal ionization cavity source for mass spectrometry. *Journal*
791 *of the American Society for Mass Spectrometry* 10, 1008–1015. [https://doi.org/10.1016/s1044-](https://doi.org/10.1016/s1044-0305(99)00065-3)
792 [0305\(99\)00065-3](https://doi.org/10.1016/s1044-0305(99)00065-3)
- 793 Edwards, R.L., Chen, J.H., Wasserburg, G.J., 1987. $^{238}\text{U}/^{234}\text{U}$ / $^{230}\text{Th}/^{232}\text{Th}$ systematics and the precise
794 measurement of time over the past 500,000 years. *Earth and planetary science letters* 81, 175–192.
795 [https://doi.org/10.1016/0012-821x\(87\)90154-3](https://doi.org/10.1016/0012-821x(87)90154-3)
- 796 Fantle, M.S., Bullen, T.D., 2009. Essentials of iron, chromium, and calcium isotope analysis of natural
797 materials by thermal ionization mass spectrometry. *Chemical Geology* 258, 50–64.
798 <https://doi.org/10.1016/j.chemgeo.2008.06.018>
- 799 Garçon, M., Boyet, M., Carlson, R.W., Horan, M.F., Auclair, D., Mock, T.D., 2018. Factors influencing
800 the precision and accuracy of Nd isotope measurements by thermal ionization mass spectrometry.
801 *Chemical Geology* 476, 493–514. <https://doi.org/10.1016/j.chemgeo.2017.12.003>
- 802 Habfast, K., 1983. Fractionation in the thermal ionization source. *International Journal of Mass*
803 *Spectrometry and Ion Physics* 51, 165–189. [https://doi.org/10.1016/0020-7381\(83\)85004-9](https://doi.org/10.1016/0020-7381(83)85004-9)
- 804 Harper, C.L., Jacobsen, S.B., 1992. Evidence from coupled ^{147}Sm – ^{143}Nd and ^{146}Sm – ^{142}Nd
805 systematics for very early (4.5-Gyr) differentiation of the Earth's mantle. *Nature* 360, 728–732.
806 <https://doi.org/10.1038/360728a0>
- 807 Hart, S.R., Zindler, A., 1989. Isotope fractionation laws: a test using calcium. *International Journal of*
808 *Mass Spectrometry and Ion Processes* 89, 287–301. [https://doi.org/10.1016/0168-1176\(89\)83065-](https://doi.org/10.1016/0168-1176(89)83065-4)
809 [4](https://doi.org/10.1016/0168-1176(89)83065-4)

- 1
2
3 810 Harvey, J., Baxter, E.F., 2009. An improved method for TIMS high precision neodymium isotope
4 811 analysis of very small aliquots (1–10 ng). *Chemical Geology* 258, 251–257.
5 812 <https://doi.org/10.1016/j.chemgeo.2008.10.024>
6 813 Horan, M.F., Carlson, R.W., Walker, R.J., Jackson, M.G., Garçon, M., Norman, M., 2018. Tracking
7 814 Hadean processes in modern basalts with ¹⁴²Neodymium. *Earth and planetary science letters*
8 815 484, 184–191. <https://doi.org/10.1016/j.epsl.2017.12.017>
9 816 Ingeneri, K.B., Riciputi, L.R., Hedberg, P.M.L., 2002. Preliminary Results of Uranium and Plutonium
10 817 Efficiency Measurements Using a High Efficiency Cavity Ion Source Interfaced with a Finnigan
11 818 MAT 262 Mass Spectrometer 1–6.
12 819 Jacobsen, S.B., Wasserburg, G.J., 1984. Sm-Nd isotopic evolution of chondrites and achondrites, II. *Earth*
13 820 *and planetary science letters* 67, 137–150. [https://doi.org/10.1016/0012-821x\(84\)90109-2](https://doi.org/10.1016/0012-821x(84)90109-2)
14 821 Johnson, P.G., Bolson, A., Henderson, C.M., 1973. A high temperature ion source for isotope separators.
15 822 *Nuclear Instruments and Methods* 106, 83–87. [https://doi.org/10.1016/0029-554x\(73\)90049-9](https://doi.org/10.1016/0029-554x(73)90049-9)
16 823 Kirchner, R., 1981. Progress in ion source development for on-line separators. *Nuclear Instruments and*
17 824 *Methods in Physics Research A* 186, 275–293. [https://doi.org/10.1016/0029-554x\(81\)90916-2](https://doi.org/10.1016/0029-554x(81)90916-2)
18 825 Koornneef, J.M., Nikogosian, I., Bergen, M.J. van, Smeets, R., Bouman, C., Davies, G.R., 2015. TIMS
19 826 analysis of Sr and Nd isotopes in melt inclusions from Italian potassium-rich lavas using
20 827 prototype 1013Ω amplifiers. *Chemical Geology* 397, 14–23.
21 828 <https://doi.org/10.1016/j.chemgeo.2015.01.005>
22 829 Krajčó, J., Varga, Z., Yalcintas, E., Wallenius, M., Mayer, K., 2014. Application of neodymium isotope
23 830 ratio measurements for the origin assessment of uranium ore concentrates. *Talanta* 129, 499–504.
24 831 <https://doi.org/10.1016/j.talanta.2014.06.022>
25 832 Li-hua, Z., Hu, D., Guan-yi, W., Zhi-ming, L., Chang-hai, W., Xue-song, L., Guo-qing, Z., Yong-yang,
26 833 S., Zi-bin, Z., 2011. A new, ohmic-heating based thermal ionization cavity source for mass
27 834 spectrometry. *International Journal of Mass Spectrometry* 305, 45–49.
28 835 <https://doi.org/10.1016/j.ijms.2011.05.015>
29 836 Loveless, A.J., Russell, R.D., 1969. A strong-focussing lens for mass spectrometer ion sources 257–266.
30 837 Lugmair, G.W., Marti, K., 1977. SmNdPu timepieces in the Angra dos Reis meteorite. *Earth and*
31 838 *Planetary Science Letters* 35, 273–284. [https://doi.org/10.1016/0012-821X\(77\)90131-5](https://doi.org/10.1016/0012-821X(77)90131-5)
32 839 Luguët, A., Nowell, G.M., Pearson, D.G., 2008. ¹⁸⁴O/¹⁸⁸O and ¹⁸⁶O/¹⁸⁸O measurements by
33 840 Negative Thermal Ionisation Mass Spectrometry (N-TIMS): Effects of interfering element and
34 841 mass fractionation corrections on data accuracy and precision. *Chemical Geology, Highly*
35 842 *Siderophile Element Geochemistry* 248, 342–362. <https://doi.org/10.1016/j.chemgeo.2007.10.013>
36 843 Maden, C., Baur, H., Fauré, A.-L., Hubert, A., Pointurier, F., Bourdon, B., 2016. Determination of
37 844 ionization efficiencies of thermal ionization cavity sources by numerical simulation of charged
38 845 particle trajectories including space charge. *International Journal of Mass Spectrometry* 405, 1–11.
39 846 <https://doi.org/10.1016/j.ijms.2016.05.013>
40 847 Maden, C., Trinquier, A., Fauré, A.-L., Hubert, A., Pointurier, F., Rickli, J., Bourdon, B., 2018. Design of
41 848 a Prototype Thermal Ionization Cavity Source intended for Isotope Ratio Analysis. *International*
42 849 *Journal of Mass Spectrometry* 434, 70–80. <https://doi.org/10.1016/j.ijms.2018.09.006>
43 850 Marks, N.E., Borg, L.E., Hutcheon, I.D., Hutcheon, I.D., Jacobsen, B., Clayton, R.N., Clayton, R.N.,
44 851 2014. Samarium–neodymium chronology and rubidium–strontium systematics of an Allende
45 852 calcium–aluminum-rich inclusion with implications for ¹⁴⁶Sm half-life. *Earth and planetary*
46 853 *science letters* 405, 15–24. <https://doi.org/10.1016/j.epsl.2014.08.017>
47 854 Mundl, A., Touboul, M., Jackson, M.G., Day, J.M.D., Kurz, M.D., Lekic, V., Helz, R.T., Walker, R.J.,
48 855 2017. Tungsten-182 heterogeneity in modern ocean island basalts. *Science* 356, 66–69.
49 856 <https://doi.org/10.1126/science.aal4179>
50 857 Peters, B.J., Carlson, R.W., Day, J.M.D., Horan, M.F., 2018. Hadean silicate differentiation preserved by
51 858 anomalous ¹⁴²Nd/¹⁴⁴Nd ratios in the Réunion hotspot source. *Nature* 555, 89–93.
52 859 <https://doi.org/10.1038/nature25754>
53
54
55
56
57
58
59
60

- 1
2
3 860 Reimink, J.R., Chacko, T., Carlson, R.W., Shirey, S.B., Liu, J., Stern, R.A., Bauer, A.M., Pearson, D.G.,
4 861 Heaman, L.M., Heaman, L.M., 2018. Petrogenesis and tectonics of the Acasta Gneiss Complex
5 862 derived from integrated petrology and ^{142}Nd and ^{182}W extinct nuclide-geochemistry. *Earth and*
6 863 *planetary science letters* 494, 12–22. <https://doi.org/10.1016/j.epsl.2018.04.047>
7 864 Riciputi, L.R., Ingeneri, K.B., Hedberg, P.M.L., 2003. Enhanced ionization efficiency using the high
8 865 efficiency cavity source implemented on a magnetic sector TIMS. *Advances in destructive and*
9 866 *non-destructive analysis for environmental monitoring and nuclear forensics. Proceedings of an*
10 867 *international conference.*
11 868 Russell, W.A., Papanastassiou, D.A., Tombrello, T.A., 1978. Ca isotope fractionation on the Earth and
12 869 other solar system materials. *Geochimica et Cosmochimica Acta* 42, 1075–1090.
13 870 [https://doi.org/10.1016/0016-7037\(78\)90105-9](https://doi.org/10.1016/0016-7037(78)90105-9)
14 871 Saji, N.S., Wielandt, D., Paton, C., Bizzarro, M., 2016. Ultra-high-precision Nd-isotope measurements of
15 872 geological materials by MC-ICPMS. *Journal of Analytical Atomic Spectrometry* 31, 1490–1504.
16 873 <https://doi.org/10.1039/c6ja00064a>
17 874 Sato, T.K., Asai, M., Borschevsky, A., Stora, T., Sato, N., Kaneya, Y., Tsukada, K., Düllmann, C.E.,
18 875 Eberhardt, K., Eliav, E., Ichikawa, S., Kaldor, U., Kratz, J.V., Miyashita, S., Nagame, Y., Ooe,
19 876 K., Osa, A., Renisch, D., Runke, J., Schädel, M., Thörle-Pospiech, P., Toyoshima, A., Trautmann,
20 877 N., 2015. Measurement of the first ionization potential of lawrencium, element 103. *Nature* 520,
21 878 209–211. <https://doi.org/10.1038/nature14342>
22 879 Shields, W.R., 1966. NBS Technical Note 277: Analytical Mass Spectrometry Section: Instrumentation
23 880 and Procedures for Isotopic Analysis. U.S. Department of Commerce, National Bureau of
24 881 Standards.
25 882 Trinquier, A., Maden, C., Fauré, A.-L., Hubert, A., Pointurier, F., Bourdon, B., Schönbachler, M., 2019.
26 883 More than 5% Ionization Efficiency by Cavity Source Thermal Ionization Mass Spectrometry for
27 884 U Sub-ng Amounts. *Analytical Chemistry* 91, acs.analchem.9b00849.
28 885 <https://doi.org/10.1021/acs.analchem.9b00849>
29 886 Upadhyay, D., Scherer, E.E., Mezger, K., 2008. Fractionation and mixing of Nd isotopes during thermal
30 887 ionization mass spectrometry: implications for high precision $^{142}\text{Nd}/^{144}\text{Nd}$ analyses. *J. Anal. At.*
31 888 *Spectrom.* 23, 561–8. <https://doi.org/10.1039/b715585a>
32 889 Wayne, D.M., Hang, W., McDaniel, D.K., Fields, R.E., Rios, E., Majidi, V., 2001. A linear time-of-flight
33 890 mass analyzer for thermal ionization cavity mass spectrometry. *Spectrochimica Acta Part B:*
34 891 *Atomic Spectroscopy* 56, 1175–1194. [https://doi.org/10.1016/s0584-8547\(01\)00207-5](https://doi.org/10.1016/s0584-8547(01)00207-5)
35 892
36
37
38
39
40
41
42
43
44
45
46
47
48
49
50
51
52
53
54
55
56
57
58
59
60